Published in final edited form as:
Adv Funct Mater. 2008 December 22; 18(24): 3972–3980. doi:10.1002/adfm.200801215.

Biological assemblies provide novel templates for the synthesis of hierarchical structures and facilitate cell adhesion**

Sivakumar Gajjeraman*, **Gen He***, **Karthikeyan Narayanan**, and **Anne George*****
Department of Oral Biology, University of Illinois at Chicago, Chicago, IL, 60612, USA.

Abstract

Mechanical mismatch and the lack of interactions between implants and the natural tissue environment are the major drawbacks in bone tissue engineering. Biomaterials mimicking the self-assembly process and the composition of the bone matrix should provide new route for fabricating biomaterials possessing novel osteoconductive and osteoinductive properties for bone repair. In the present study, we employ bio-inspired strategies to design *de novo* self-assembled chimeric protein hydrogels comprising leucine zipper motifs flanked by dentin matrix protein 1 domain, which was characterized as a mineralization nucleator. Results showed that this chimeric protein could function as a hydroxyapatite nucleator in pseudo-physiological buffer with the formation of highly oriented apatites similar to biogenic bone mineral. It could also function as an inductive substrate for osteoblast adhesion, promote cell surface integrin presentation and clustering, and modulate the formation of focal contacts. Such biomimetic “bottom-up” construction with dual osteoconductive and osteoinductive properties should open new avenues for bone tissue engineering.

Mechanical mismatch and the lack of interactions between implants and the natural tissue environment are the major drawbacks in bone tissue engineering. Biomaterials mimicking the self-assembly process and the composition of the bone matrix should provide new route for fabricating biomaterials possessing novel osteoconductive and osteoinductive properties for bone repair. In the present study, we employ bio-inspired strategies to design *de novo* self-assembled chimeric protein hydrogels comprising leucine zipper motifs flanked by dentin matrix protein 1 domain, which was characterized as a mineralization nucleator. Results showed that this chimeric protein could function as a hydroxyapatite nucleator in pseudo-physiological buffer with the formation of highly oriented apatites similar to biogenic bone mineral. It could also function as an inductive substrate for osteoblast adhesion, promote cell surface integrin presentation and clustering, and modulate the formation of focal contacts. Such biomimetic “bottom-up” construction with dual osteoconductive and osteoinductive properties should open new avenues for bone tissue engineering.

Keywords

dentin matrix protein 1; leucine zipper; self-assembly; cell adhesion; mineralized matrix

This work was supported by NIH grant DE 16533 Supporting Information is available online from Wiley InterScience.

***To whom correspondence should be addressed. Anne George, Department of Oral Biology, University of Illinois at Chicago, Chicago, IL 60612 (USA), anneg@uic.edu, Tel.: 312-413-0738; Fax: 312-996-6044.
*Both contributed equally to this work

1. Introduction

Template directed synthesis has produced a diverse range of new inorganic-based materials with unique mechanical properties. [1–4] One promising strategy is to use molecular structure to direct nanocrystal nucleation and crystal growth. To this end, protein-based nanostructures provide functional building blocks for the development of multi-functional materials. [5–11] Novel materials can be synthesized by emulating the self-assembly strategy that nature does. Self-assembly would allow controlled organization of the organic/inorganic interface based on molecular recognition elements, resulting in hierarchical organization with desirable properties at multiple length scales. Nature has provided a diversity of peptide motifs that can serve as building blocks capable of self-assembling into macroscale materials with pre-defined structure and properties. [12] The properties of such motifs can be exploited for the rational design of novel materials, tailored to the requirements of specific biological applications. [6,13] Developing such templates is necessary for the development of hierarchically structured materials like bone and dentin. [5,6]

One of the best studied self-assembling motifs is leucine zipper (coiled-coil motif). [14–16] Petka et al. [17] designed a tri-block artificial protein with an alanylglycine-rich coil between two terminal leucine zipper (LZ) motifs. Such a strategy is particularly interesting because multiple bioactive motifs can be potentially incorporated into the construct and the LZ self-assembling properties will be unaffected if designed appropriately.

In the present study, we show that self-assembling LZ polypeptides can be designed to accommodate motifs from the hydroxyapatite nucleating domain and cell adhesive motifs of dentin matrix protein 1 (DMP1). [18,19] Although, DMP1 was initially isolated from the dentin matrix and was thought to be unique to dentin and named accordingly, it has now been found to be present in all mineralized tissues of the vertebrate system. The C-terminal polypeptide of DMP1 contains the HAP nucleating domain as well as an RGD motif for cell-adhesion, which makes it a highly desirable polypeptide for *in-vivo* applications requiring calcified tissue formation. [18,19]

From the structural and functional diversity of natural proteins, we devised a modular design that enables controlled crystalline hydroxyapatite deposition as well as provide appropriate stimulation for cellular activity. The template is synthesized using a double stranded DNA fragment coding for leucine zipper motif based on the reported sequences.[17] Extra N and C-caps were incorporated to initiate and terminate the α-helix correctly for proper protein folding. Through multiple PCR amplification and DNA recombination strategies a cDNA fragment coding for C-terminal DMP1 (amino acid residues 328–360 containing the RGD motif and the functional domain for apatite nucleation [18]) was also incorporated between the two LZ domains. This plasmid was transformed into BL-21 E.coli and expressed as GST-fused recombinant protein. Thus, integration of biological self-organization and inorganic assembly components is important to synthesize complex materials that exhibit order from the molecular to the macroscopic scale.

2. Results and Discussion

2.1. Characterization of the chimeric protein

The apparent molecular weight of the chimeric protein LZ-DMP1 was ~25kDa [Fig 1A] and consists of 2 short leucine zipper motives on either ends with the C-terminal DMP1 at the centre of the molecule [Fig 1B]. The sequence was verified by MALDI-TOF spectroscopy [Fig 1C].

2.2 Characterization of the self-assembling property of LZ-DMP1

CD Spectroscopy—The folding of LZ-DMP1 under physiological conditions was characterized by circular dichroism spectroscopy (CD). For comparison, CD analysis was performed on leucine zipper protein without DMP1 (LZ) and the C-terminal DMP1 (C-DMP1). The CD profiles of both LZ and LZ-DMP1 shows the presence of α-helix with negative absorption at 211 and 222 nm [Fig 2 (i)], while C-DMP1 had a random coil conformation with negative absorption at 200 nm and in the presence of calcium a shoulder was observed at 227nm indicating the presence of β-sheet [Fig 2 (ii)]. The CD profile of LZ-DMP1 in the presence of 2.5 and 5mM Ca^{2+} was a combination of the structural components of both LZ and that of C-DMP1 [Fig 2 (i)]. Physiological pH was determined to be optimum as the chimeric protein had characteristics of both the α-helix and the β-sheet (Supplementary Figure 1). These results established that the designed leucine zipper peptide maintains a native-like helical conformation and the C-terminal DMP1 domain in the chimeric protein could fold independently and adopt a β-sheet conformation in the presence of calcium and at neutral pH.

Atomic Force Microscopy—The self-assembly process was monitored by Atomic force microscopy (AFM). AFM imaging of the protein coated surfaces are shown in Fig 3 which contain representative images. As expected, results in Fig 3 (i) show that LZ can self-assemble from monomeric (25nm) to globular structures in the presence of calcium. However, the chimeric protein LZ-DMP1 can undergo hierarchical self-assembly forming nanometer-sized clusters within 3 hrs to more compact globular aggregates of ~ 200nm sized particles within 6 hrs [Fig 3 (ii)]. At 24hrs of incubation, LZ-DMP1 could further self-assemble to form long fibrillar structures. These fibrils, radiating from the centre can entwine to form a network of nanofibrous scaffolds [Fig 3 ii]. Thus, in the presence of Ca^{2+} intermolecular bridging interactions led to the enhanced self-assembly of LZ-DMP1.

2.3 *In-vitro* nucleation assay and characterization of the calcium phosphate deposits

In order to determine if LZ-DMP1 can direct ordered hydroxyapatite (HAP) deposition, *in-vitro* nucleation experiments were conducted. Nucleation experiments were performed on a glass slide coated with LZ and LZ-DMP1 as published earlier. [19] The presence of protein on the glass plate was visualized by using FITC labeled LZ [Fig 4A (i)] and LZ-DMP1 [Fig4B]. With LZ template the calcium phosphate deposits appeared amorphous at the end of 8 days of growth [Fig 4A (ii)]. The amorphous nature was confirmed by the diffused ring pattern from electron diffraction data [Fig 4A (iii)], a predominant band at 949 cm^{-1} in the Raman spectra [Fig 4A (iv) and a Ca/P ratio of 1.48 by EDX [Fig 4A (v)]. However, with LZ-DMP1, calcium phosphate deposits harvested at the end of 2, 4, 6 & 8 days demonstrated a gradual transformation from amorphous calcium phosphate (day 2) to crystalline, needle-shaped HAP crystals (day 8) [Fig 4B]. High resolution transmission electron microscopy (HRTEM) and the corresponding selected area electron diffraction (SAED) demonstrated that the crystals adopted preferential alignment along the c-axis mimicking the apatite arrangement in mineralized bone and dentin [Fig 5A i &ii]. The lattice spacing of 0.345nm indicated that the long axis of the HAP crystal corresponds to the (002) lattice plane of HAP [Fig 5A (iii)]. The crystalline nature of the HAP deposits was further confirmed by XRD and Raman spectroscopy. XRD analysis demonstrated sharp intensities of the peaks at 25.6° and 31.6° corresponding to a preferential alignment along (002) and (211) growth planes [Fig 5B (i)]. Raman spectra in Fig 5B (ii) demonstrated that the calcium phosphate deposits at the end of 8 days of growth period was crystalline HAP. Symmetric stretch of the phosphate at 960 cm^{-1} confirmed the presence of crystalline HAP. The shift of the phosphate band from 950 cm^{-1} for samples harvested at day 2 to 960 cm^{-1} at the end of day 8 confirmed the conversion of amorphous calcium phosphate to crystalline HAP. Elemental analysis by energy dispersive X-ray (EDX) [Fig5B (iii)] indicated that the Ca/P

ratio increased from 1.47 to 1.69 with progression in the transformation and maturation process. The transformation of the initial amorphous precursor phase can be possibly modulated by crystal-protein interactions resulting in its hydrolysis to apatite. Thermodynamically, the driving force for the HAP formation would be the change in Gibbs free energy ΔG for the transfer from the supersaturated solution to the equilibrium state. Thus, highly ordered LZ-DMP1 template could control the formation of crystalline apatite by molecular recognition mechanisms between LZ-DMP1 template and the apatite surface.

2.4 ToF-SIMS analysis

To demonstrate the molecular mechanism by which oriented HAP is deposited on the LZ-DMP1 template, time-of-flight secondary ion mass spectroscopy (TOF-SIMS) was used to map the surface distribution of calcium and phosphate ions along with the amino acid residue associated with Ca^{2+}. Examination of the elemental composition of the mineralized surface suggests that the intrinsic intensity of Ca^{2+} ion signal spalled from the surface was more intense in the LZ-DMP1 samples (Fig 6ii) when compared with the LZ polypeptide by itself [Fig 6 (i)]. In the calcium-dominant region, phosphate ions seemed to be enriched. Similar results were obtained using bovine dentin slice as a positive control (Supplementary Figure 2). Interestingly, surface ion etching confirmed that the predominant amino acid in contact with the crystal surface is glutamic acid [Fig 6 (iii) &(iv)]. Thus, the self-assembled monolayer containing carboxylates appeared to bridge calcium and phosphate ions during *de-novo* hydroxyapatite formation. Examination of the amino acid sequence for C-DMP1 shows several sequence domains that contain an abundance of glutamic acid. The carboxylate groups in glutamic acid might increase the charge density resulting in high affinity between the calcium ions and the carboxylates resulting in epitaxial nucleation and outward growth of platy crystals of HAP. Thus, molecular recognition mechanisms between the aligned carboxylates on the self-assembled template and the mineral surface might contribute to the orientational specificity of HAP.

2.5 Characterization of the cellular response

Incorporation of biomolecular recognition domains into a biomaterial is necessary for providing molecular features to direct cellular activity for optimal *in-vivo* integration and function. In the present study the C-DMP1 fragment contains an RGD motif which could be exploited to deliver instructive signals from the LZ-DMP1 template. Cell surface integrins are the major receptors that mediate communications between cells and the extracellular matrix across the plasma membrane. Fibronectin is one such major ECM protein that activates integrins via its RGD motif. [20,21] Anti-fibronectin antibodies have been shown to inhibit steady-state expression of genes associated with osteoblast differentiation, which specifically emphasize the importance of incorporation of bioactive molecules into biomaterials for bone tissue regeneration. [22] To assess the ability of the LZ-DMP1 macromolecule to affect cellular behavior, we examined attachment morphology, proliferation and activation of adhesion components. The first experiment was to determine the attachment response of pre-osteoblastic MC3T3-E1 cells plated on glass cover-slips pre-coated with a monolayer of LZ-DMP1. Results in Fig 7 A show that cells adhered and proliferated well on LZ-DMP1coated substrate, while few cells attached on the control cover glass. In order to determine if cell adhesion is mediated by focal adhesion complexes, cells were seeded on LZ-DMP1 coated glass coverslips or on blank glass coverslips. After 48hrs the cells were stained for actin using a fluorescent dye and the focal adhesion sites were identified using immuno-fluorescently labeled paxillin. Results in Fig 7C demonstrate that LZ-DMP1 supports cell-adhesion by promoting assembly of focal adhesion sites. This was accompanied by lamellipodial protrusion, which is an indication of cell migration [Fig 7B]. Thus, the LZ-DMP1 template can provide cues to appropriately direct cellular activity.

Cell adhesion to the extracellular matrix is mediated by integrins (adhesion receptors) which is composed of α subunit associated with a β subunit. [23] Binding of cells to the matrix promotes integrin clustering, which in turn recruits actin filaments and directs focal adhesion complex formation. In order to confirm integrin-RGD binding was responsible for the attachment, β1 integrin expression levels of MC3T3-E1 grown on various concentrations of LZ-DMP1 protein after surface biotinylation was examined. Cell lysates were immunoprecipitated with β1 integrin antibody. Western blot analysis using Extravidin (Sigma) showed that the cell surface β1 increased in a dose-dependent manner [Fig 7E]. This result was further confirmed by cell surface immuno-fluorescent labeling with anti-β1 integrin antibody, which indicated that both the expression level and the β1 integrin clustering were enhanced with higher concentrations of the protein [Fig 7D]. Interaction of integrin with such templates can control an assortment of biological processes.

3. Conclusions

Bone a biological composite of organic and inorganic phases has a microstructure that provides an unusual combination of toughness and fracture resistance. Using the principle of biomimicry, we demonstrate a novel strategy for synthesizing *de novo* cell interactive templates, which can also promote template-driven mineralization of crystalline apatites for hard tissue regeneration. The self-assembled biomaterial can induce and assemble mineral formation at the nanoscale level. It can also modulate cell-matrix dialogues, which is necessary for cellular differentiation and matrix formation. Furthermore, biomaterials with multiple ligands can be easily built based on current strategy by mixing constructs sharing the same self-assembling motif resulting in biomolecular templates with a highly ordered display of versatile functional groups critical for cellular and mineralization functions. Overall, self-assembled peptide based biomaterials have intrinsic advantages such as being biodegradable, biocompatible and possess minimal biotoxicity. The current “bottom-up” fabrication approach should allow precise tailoring of the material properties for various applications.

4. Materials and Methods

Plasmid construction, recombinant protein expression and purification

Double stranded DNA fragment (GGTTCTTCTGGTGAACTGGAAAACGAAGTTGC TCAGCTGGAACGTGAAGTACGTTCCCTGGAAGACGAAGCTGCAGAGCTGGAAC A GAAAGTTTCTCGCCTGAAAAACGAAATCGAAGACCTGAAAGCTGAACC GGGTTCT) coding for leucine zipper motif (G S S G E L E N E V A Q L E R E V R S L E D E A A E L E Q K V S R L K N E I E D L K A E P G S) was synthesized using an ABI 3900 High-Throughput DNA Synthesizer. Multiple restriction enzyme sites were added to the ends of the DNA fragment by PCR amplifying using the corresponding primers. Afterwards, the fragment with Bam HI/EcoR I/Xho I/Not I sites was inserted to the Bam HI/ Not I site of the pGEX4T-3 vector (Amersham Biosciences). In the second step the DNA fragment with Bam HI/EcoRI site was incorporated into the pGEX4T-3 vector containing one leucine zipper DNA fragment in it. In the third step cDNA fragment coding for C-DMP1 protein residues 328–360 (does not contain the RGD domain) was amplified with EcoR I/ Xho I sites and inserted into the plasmid generated containing two leucine zipper DNA fragments. Thus, a plasmid was generated comprising two leucine zipper DNA oligonucleotides flanked by one cDNA fragment coding for C-DMP1 (Fig. 1a). The plasmid was transformed into BL21 *E. coli* (Invitrogen) and expressed as GST fused recombinant protein. The recombinant protein was purified according to the manufacturer’s protocol and cleaved with thrombin to release the LZ-DMP1 protein. The residual thrombin was cleared by passing the recombinant protein through a benzamidine sepharose column. Constructs

comprising only two LZ fragments were also expressed and served as controls. C-DMP1 recombinant was purified as described before (7).

Characterization of the chimeric protein by SDS-PAGE analysis and MALDI-TOF-MS peptide mapping

The purity and molecular weight of the each purified proteins were verified by Sodium dodecyl sulfate polyacrylamide gel electrophoresis (SDS-PAGE). The recombinant protein was further characterized by MALDI-TOF-MS peptide mapping. The LZ-DMP1-LZ protein was excised from the gel strip and subjected to trypsin in-gel digestion. After 24 hours the peptides were extracted and the samples were spotted onto a 96X2 – position MALDI-TOF target and analyzed by a positive-ion Voyager DE-PRO mass spectrometer (Applied Biosystem, Foster City, CA) equipped with nitrogen laser. Peptide mass maps were measured at an instrument resolution of 10,000 in a reflector mode with delayed extraction over the m/z ratio 700–4000Da. Samples were externally calibrated. Protein prospector software (http://prospector.ucsf.edu) was used to analyze the MS results.

Characterization of the self-assembly characteristics of LZ-DMP1

Circular Dichroism Spectroscopy—Far-ultraviolet circular dichroism measurements were made on a JASCO J-320 spectropolarimeter using 5 mM peptide in 0.1 mM HEPES, pH 7.4, in a 1-mm path-length cell at 20 °C. Data were collected at 0.5 nm intervals at 2 nm min^{-1}. Five such runs were averaged, calculated net of buffer, and smoothened using the accompanying software program. Ellipticity measurements was normalized to the mean residue ellipticity (θ) expressed in units deg cm^2 $dmol^{-1}$. Conformational change in the presence of calcium was determined by incubating 0.1mg/ml protein solution with 5mM calcium ions overnight at 37° C and 5% CO_2. Experiments were also conducted by varying the pH of the protein samples in the presence of calcium ions. Conformational change was also monitored at pH 4,5,6,7 7.4 & 8 (using 10mM sodium citrate or 10mM HEPES). The final CD spectra of the proteins were obtained by subtracting the spectra of the appropriate buffer and smoothened using the accompanying software.

***In-vitro* Nucleation experiment—**Nucleation experiments were performed on glass substrates and these plates were prepared according to published protocols [19]. *In-vitro* mineralization experiments were performed using FITC labeled proteins coated on the treated glass plates for 2 hrs at 37°C and 5% CO_2. The presence of protein on the substrate was verified by immersing a coated plate in 10mM HEPES buffer for 2, 4, 6 & 8 days pH 7.4 and then viewed under the confocal microscope. Nucleation experiments were performed according to earlier published protocol [19].

Characterization of the deposited mineral—The mineral deposited on the substrate was characterized by powder X-ray electron diffraction (XRD), Raman spectroscopy, Scanning electron microscopy (SEM) and Transmission Electron Microscopy (TEM) and Energy Dispersive Analysis (EDX).

Scanning Electron Microscopy (SEM)—For SEM analysis, the mineralized deposit was dried through critical point drying and spread over the aluminum stub using double sticky tape and then coated with gold by a sputtering technique at a vacuum of 10^{-5} Torr.

Transmission Electron Microscopy (TEM)—JEOL 3010 transmission electron microscope was used to analyze calcium phosphates harvested from LZ and LZ-CDMP1 template. To assess the orientation, selected area electron diffraction (SAED) technique was performed. For the morphology and selected area electron diffraction studies, the minerals were ground into fine powder and separated by ultrasonic vibration in an ethanol medium

and then placed on carbon Formvar coated nickel grids. Composition of the minerals harvested from the LZ-CDMP1 template was studied using EDX (Vista model, Thermo Noran) coupled with TEM

Surface Characterization studies

Time–of-flight Secondary Ion Mass Spectrometry analysis (TOF-SIMS): The distribution and localization of calcium, phosphorous and amino acid residues before and after ion etching over an area 50μm × 50 μm (under static condition) were studied using a PHI TRIFT III TOF-SIMS apparatus (Physical Electronics). A dual beam depth profiling was carried out using 1KeV Ar^+ erosion beam rastered over an area (300μm ×300 μm) and an analysis beam (25 keV Ga^+) rastered over an area (50μm × 50 μm) in order to identify the elements present in different layers. The atomic and molecular surface constituents emitted as a result of primary ion bombardment are observed as neutral particles or as positive or negative secondary ions. The mass scales of the positive ion spectra were calibrated using: H^+, CH_3^+, $C_2H_3^+$ and $C_3H_5^+$) and the negative ion spectra were calibrated using CH^-, OH^-, and C_2H^-. Sample surfaces were cleaned by sputtering for 2 min before collecting the spectra and images. To identify the amino acid distribution, the samples were etched for one hour and based on the mass of 56 mass units for the fragment C_3H_4O the peak was assigned to glutamic acid residue.

Atomic Force Microscope (AFM)—AFM imaging method was used to demonstrate the self assembling characteristics of LZ-DMP1 and LZ control protein in the presence and absence of calcium. The proteins were used at a concentration of 0.5 mg/ml in 10mM HEPES. pH 7.4 was used. 5mM Ca^{2+} solution was mixed with 50 ul of protein solution and incubated at 37°C. Topographical images were obtained at 3 different time periods (3 hrs 6hrs and 24hrs) and the solution (20μl) was used to study the self assembling properties of the proteins. At two different time periods (6 & 24 hrs) 20 ul protein was added onto freshly cleaved mica substrate. Images were captured by using MFP-3D™ (Asylum Research) equipped with flexured scanner. Silicon cantilevers with a spring constant at 20–50 N/m and resonance frequency at 300 kHz were used for all measurements.

Cell adhesion assays and cytoskeletal arrangement—Cell attachment assays of MC3T3-E1 cells on LZ and LZ-DMP1 templates coated on glass plates were performed by coating the proteins on the glass plate. After blocking with 0.5 mg/ml heat-inactivated BSA in PBS at 37°C for 1hr, approximately 4×10^4 cells were allowed to attach overnight at 37°C. Adherent cells were imaged using a light microscope. In order to characterize the focal adhesion sites and cytoskeleton arrangement, glass coverslips were coated with self-assembled 1 mg/ml LZ-DMP1 and seeded with MC3T3-E1 cells. After 48hrs, cells were fixed with 3.8% formaldehyde, permeabilized using 1% Triton X-100 in PBS and immunofluorescently labeled with anti-paxillin antibody (BD Biosciences). The actin cytoskeleton was labeled with Oregon 514 (Invitrogen). Labeled cells were examined by Zeiss LSM 510 confocal microscopy.

In order to determine if β1 integrin was expressed and activated MC3T3-E1 cells cultured on different concentrations of LZ-DMP1 hydrogel were fixed with 3.8% formaldehyde without permeabilization and fluorescently labeled with β1 integrin antibody and examined under confocal microscopy. Alternatively, cells in culture were cell surface biotinylated using sulfo-NHS-LC-biotin (Pierce Inc.) and lysed in 50mM Tris, pH 7.5, 150mM NaCl, 1% Triton X-100, 5mM EDTA with protease inhibitors cocktail (Roche Inc.). β1 integrin was immunoprecipitated using protein G agarose beads coupled to β1 integrin antibody, separated by polyacrylamide gel electrophoresis, and blotted onto PVDF membrane. The surface β1 integrin was detected using HRP-conjugated Extravidin (Sigma).

Supplementary Material

Refer to Web version on PubMed Central for supplementary material.

References

1. Meadows PJ, Dujardin E, Hall SR, Mann S. Chem Commun (Camb). 2005:3688. [PubMed: 16027912]
2. Arico F, Chang T, Cantrill SJ, Khan SI, Stoddart JF. Chemistry. 2005; 11:4655. [PubMed: 15887196]
3. Ha C, Park CB. Biotechnol Bioeng. 2005; 90:848. [PubMed: 15803463]
4. Berl VV, Krische MJ, Huc II, Lehn JM, Schmutz M. Chemistry. 2000; 6:1938. [PubMed: 10894393]
5. He G, George A. J Biol Chem. 2004; 279:11649. [PubMed: 14699165]
6. Dettin M, Conconi MT, Gambaretto R, Pasquato A, Folin M, Di Bello C, Parnigotto PP. J Biomed Mater Res. 2002; 60:466. [PubMed: 11920671]
7. Sarikaya M, Tamerler C, Jen AK, Schulten K, Baneyx F. Nat Mater. 2003; 2:577. [PubMed: 12951599]
8. Chowdhury EH, Akaike T. Curr Gene Ther. 2005; 5:669. [PubMed: 16457655]
9. Ma H, Zin MT, Zareie MH, Kang MS, Kang SH, Kim KS, Reed BW, Behar CT, Sarikaya M, Jen AK. J Nanosci Nanotechnol. 2007; 7:2549. [PubMed: 17685271]
10. Reches M, Gazit E. J Nanosci Nanotechnol. 2007; 7:2239. [PubMed: 17663236]
11. Ryadnov MG. Biochem Soc Trans. 2007; 35:487. [PubMed: 17511635]
12. Kumar M, Sanford KJ, Cuevas WA, Du M, Collier KD, Chow N. Biomacromolecules. 2006; 7:2543. [PubMed: 16961316]
13. Bonzani IC, George JH, Stevens MM. Curr Opin Chem Biol. 2006; 10:568. [PubMed: 17011226]
14. Jerome V, Muller R. Gene Ther. 2001; 8:725. [PubMed: 11406767]
15. Liu N, Caderas G, Deillon C, Hoffmann S, Klauser S, Cui T, Gutte B. Curr Protein Pept Sci. 2001; 2:107. [PubMed: 12370019]
16. Mi L, Fischer S, Chung B, Sundelacruz S, Harden JL. Biomacromolecules. 2006; 7:38. [PubMed: 16398496]
17. Petka WA, Harden JL, McGrath KP, Wirtz D, Tirrell DA. Science. 1998; 281:389. [PubMed: 9665877]
18. Gajjeraman S, Narayanan K, Hao J, Qin C, George A. J Biol Chem. 2007; 282:1193. [PubMed: 17052984]
19. He G, Dahl T, Veis A, George A. Nat Mater. 2003; 2:552. [PubMed: 12872163]
20. Moursi AM, Damsky CH, Lull J, Zimmerman D, Doty SB, Aota S, Globus RK. J Cell Sci. 1996; 109(Pt 6):1369. [PubMed: 8799825]
21. Petrie TA, Capadona JR, Reyes CD, Garcia AJ. Biomaterials. 2006; 27:5459. [PubMed: 16846640]
22. Globus RK, Moursi A, Zimmerman D, Lull J, Damsky C. ASGSB Bull. 1995; 8:19. [PubMed: 11538547]
23. Takada Y, Ye X, Simon S. Genome Biol. 2007; 8:215. [PubMed: 17543136]

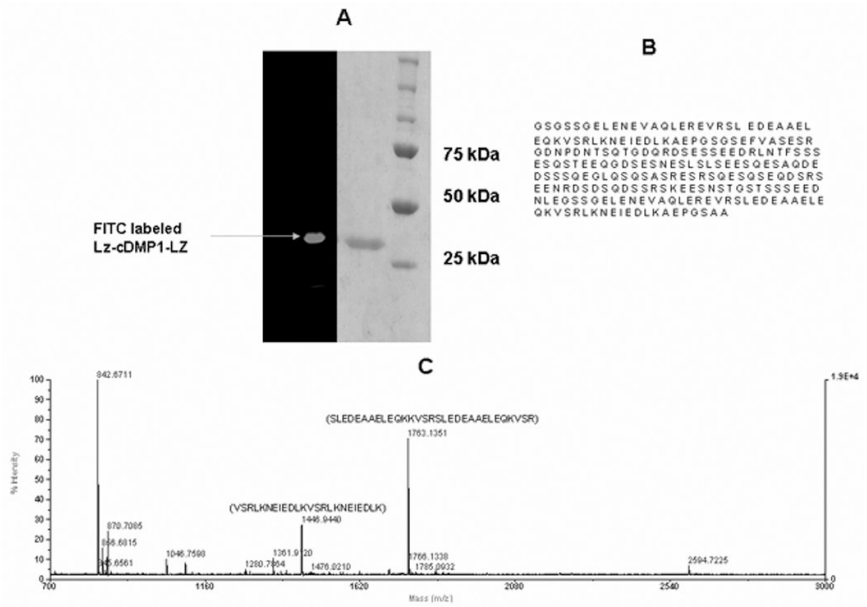

Figure 1. Characterization of the chimeric protein

A: SDS-PAGE analysis of purified recombinant LZ-CDMP1and FITC labeled LZ-CDMP1; B: Amino acid sequence of the LZ-CDMP1 protein; C: Mass spectroscopy analysis showing the sequence of the tryptic peptides obtained from the chimeric protein.

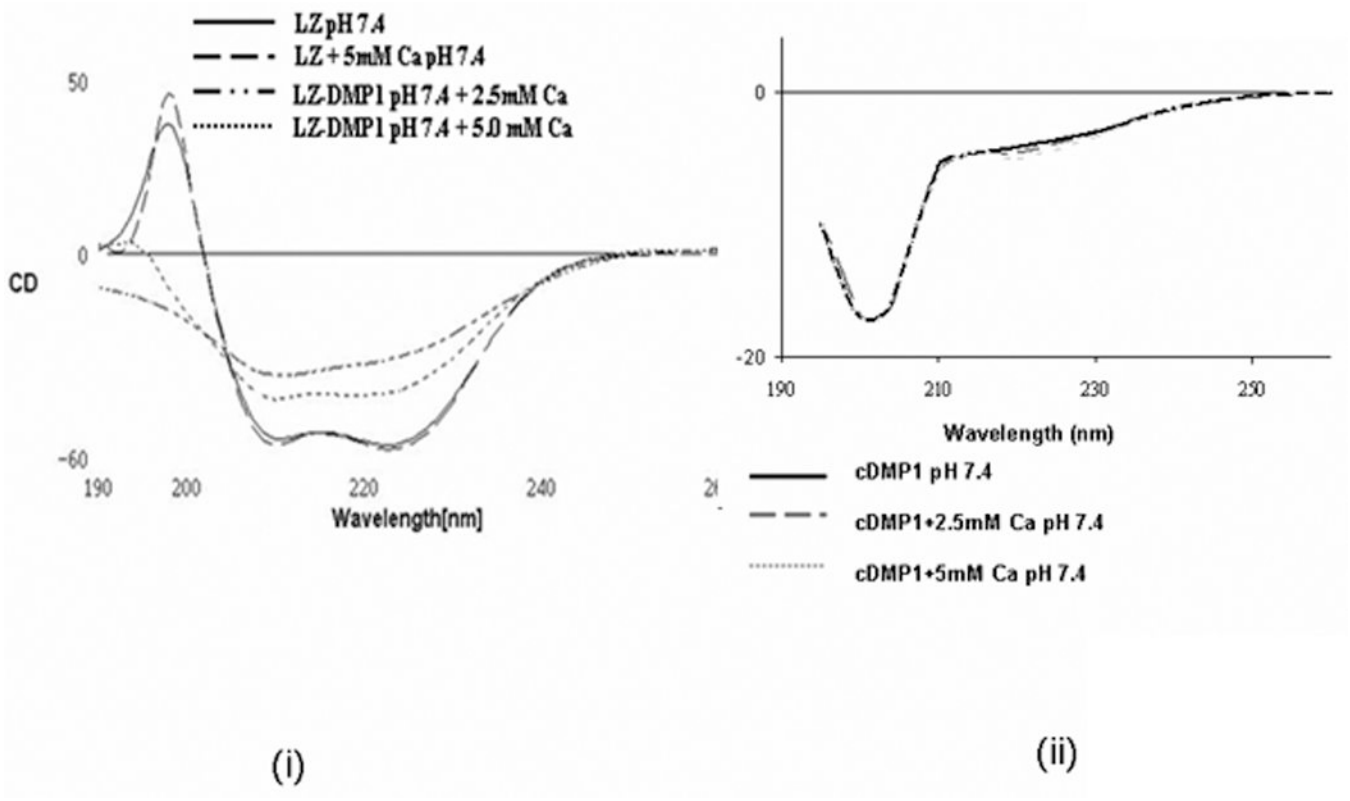

Figure 2. Conformation of LZ and LZ-DMP1 as determined by CD spectroscopy

(i) Far-ultraviolet circular dichroism (CD) spectrum of LZ and LZ-CDMP1 in 0.1mM HEPES pH7.4 in the presence and absence of 2.5 and 5mM Ca^{2+}. CD spectrum shows that the chimeric protein possess α-helix conformation with negative absorptions at 211 and 222nm, while C-DMP1 was assigned a random coil with negative absorption at 200 nm; **(ii)** CD spectra of recombinant DMP1 in the presence and absence of 2.5 and 5mM Ca^{2+}. CD spectra shows a minimum at 200 nm and a prominent shoulder at 227nm indicating the presence of β-sheet and α- helical structure.

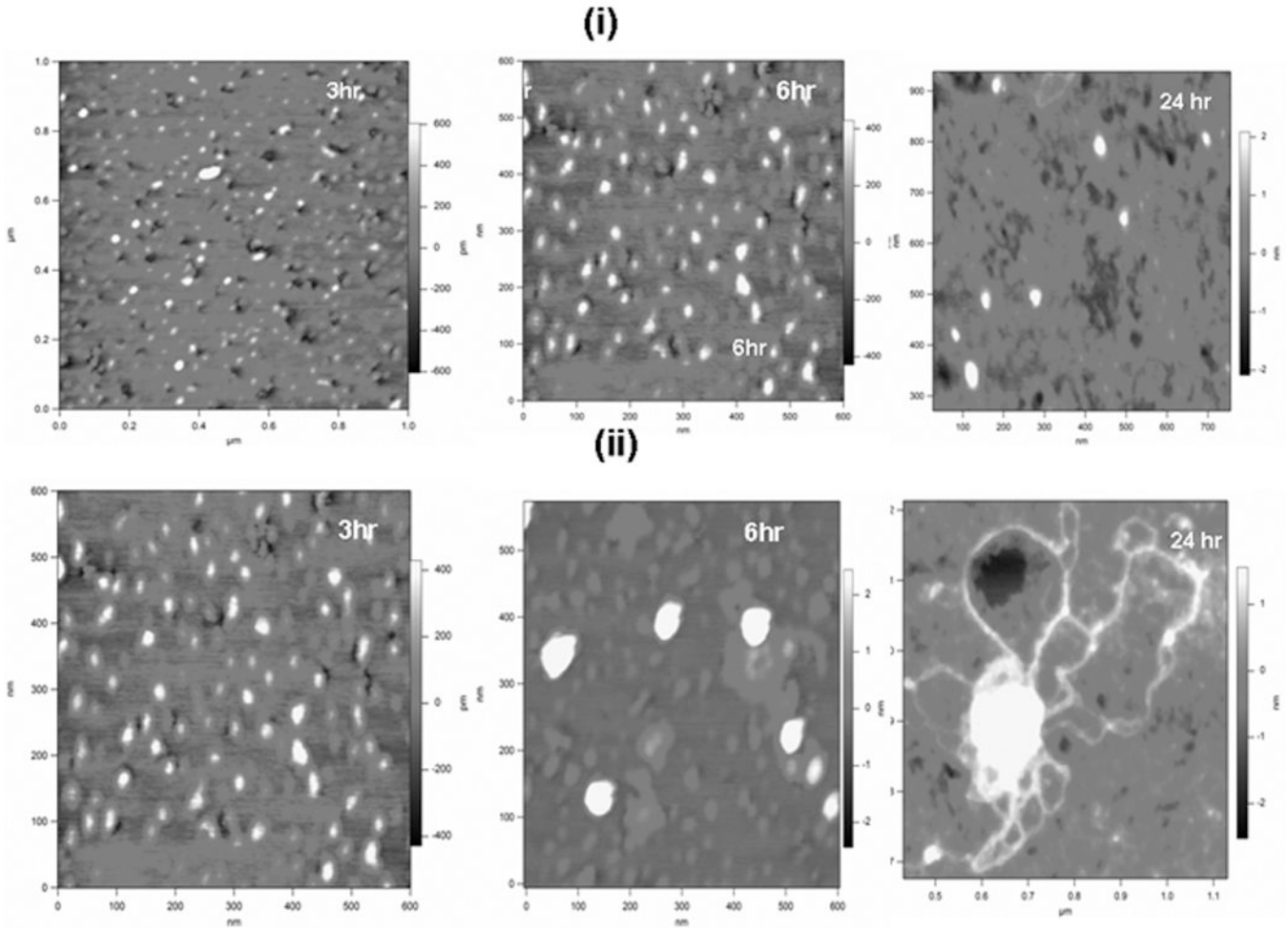

Figure 3. AFM image showing self-assembly of LZ and LZ-CDMP1in the presence of 5mM Ca^{2+}

(i) Topographic image of the self-assembly of LZ protein in the presence of 5mM Ca^{2+} at 3,6 & 24 hr; (ii) Topographic image of the self-assembly of LZ-CDMP1 in the presence of Ca^{2+} at 3,6 & 24hr.

FIG 4A

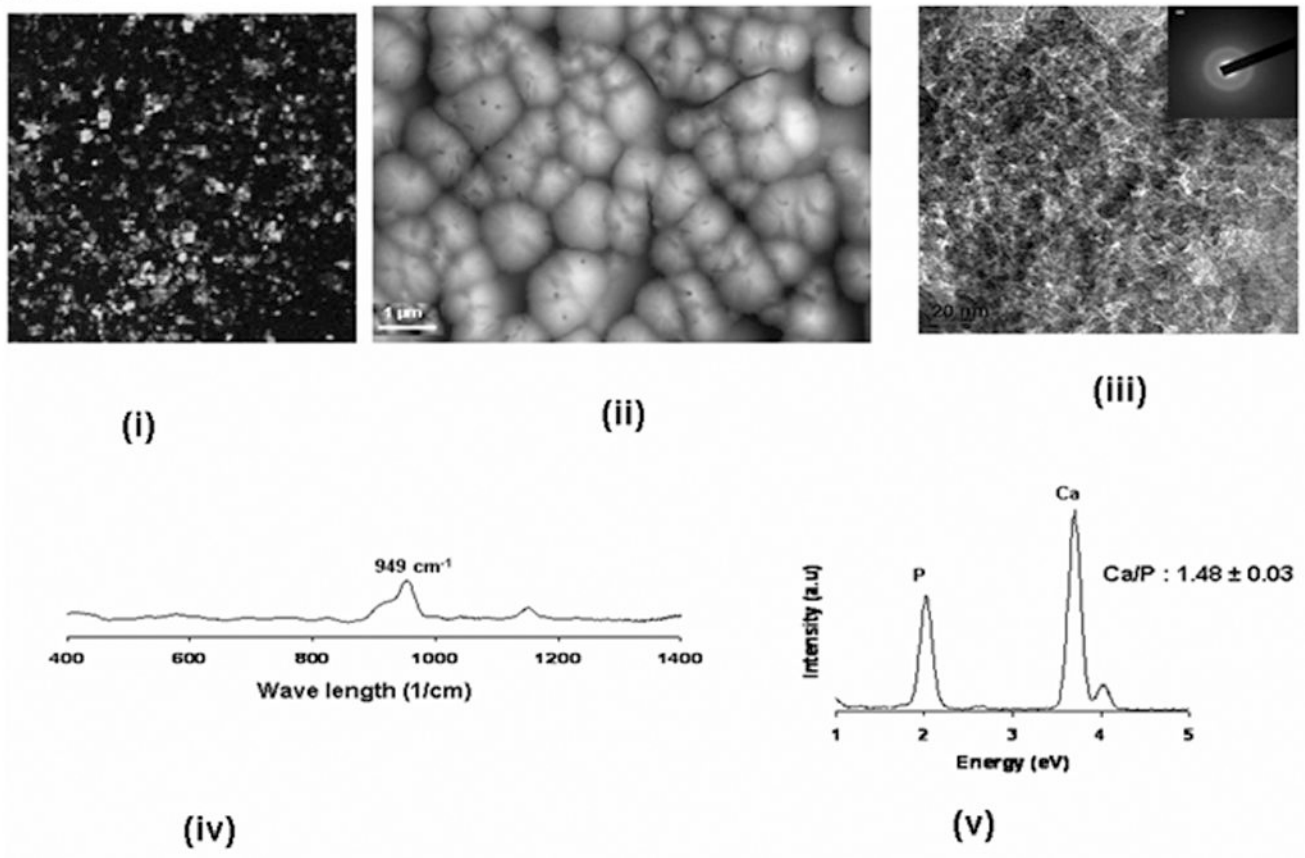

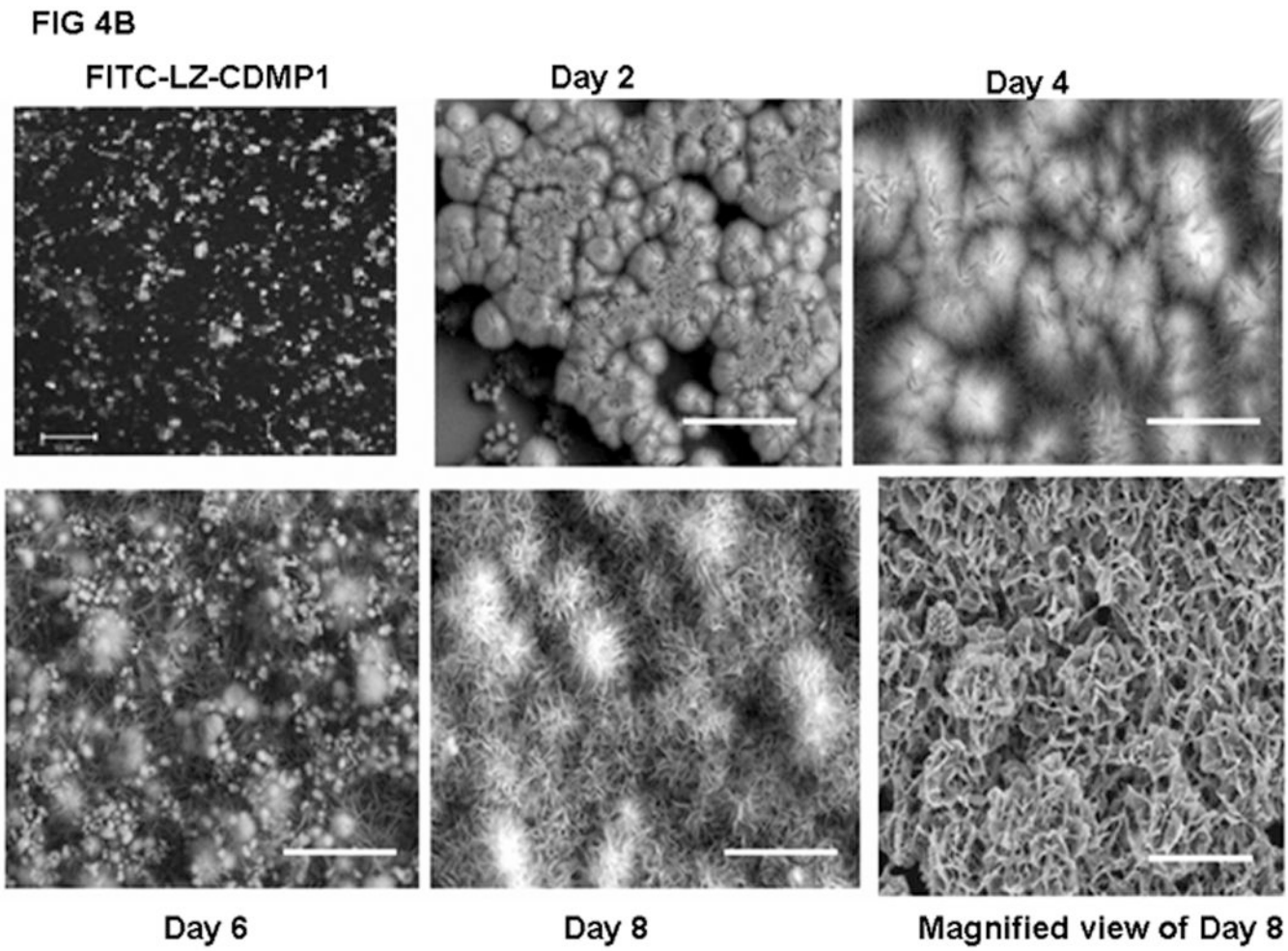

Figure 4.

A: Calcium phosphate deposition on LZ template (i) FITC-LZ coated glass plates (ii) SEM analysis of the calcium phosphate deposited after 8 days of growth period; (iii) TEM analysis showing the amorphous nature of the calcium phosphate deposits; *inset*: Electron diffraction pattern showing diffused rings confirming the amorphous nature; (iv) Raman spectra of the calcium phosphate deposit; (v) EDX spectra of amorphous calcium phosphate deposit.

B: Calcium phosphate deposition on LZ-DMP1 template: SEM analysis of CaP deposits obtained after 2, 4, 6, and 8 days of growth period.

FIG 5A

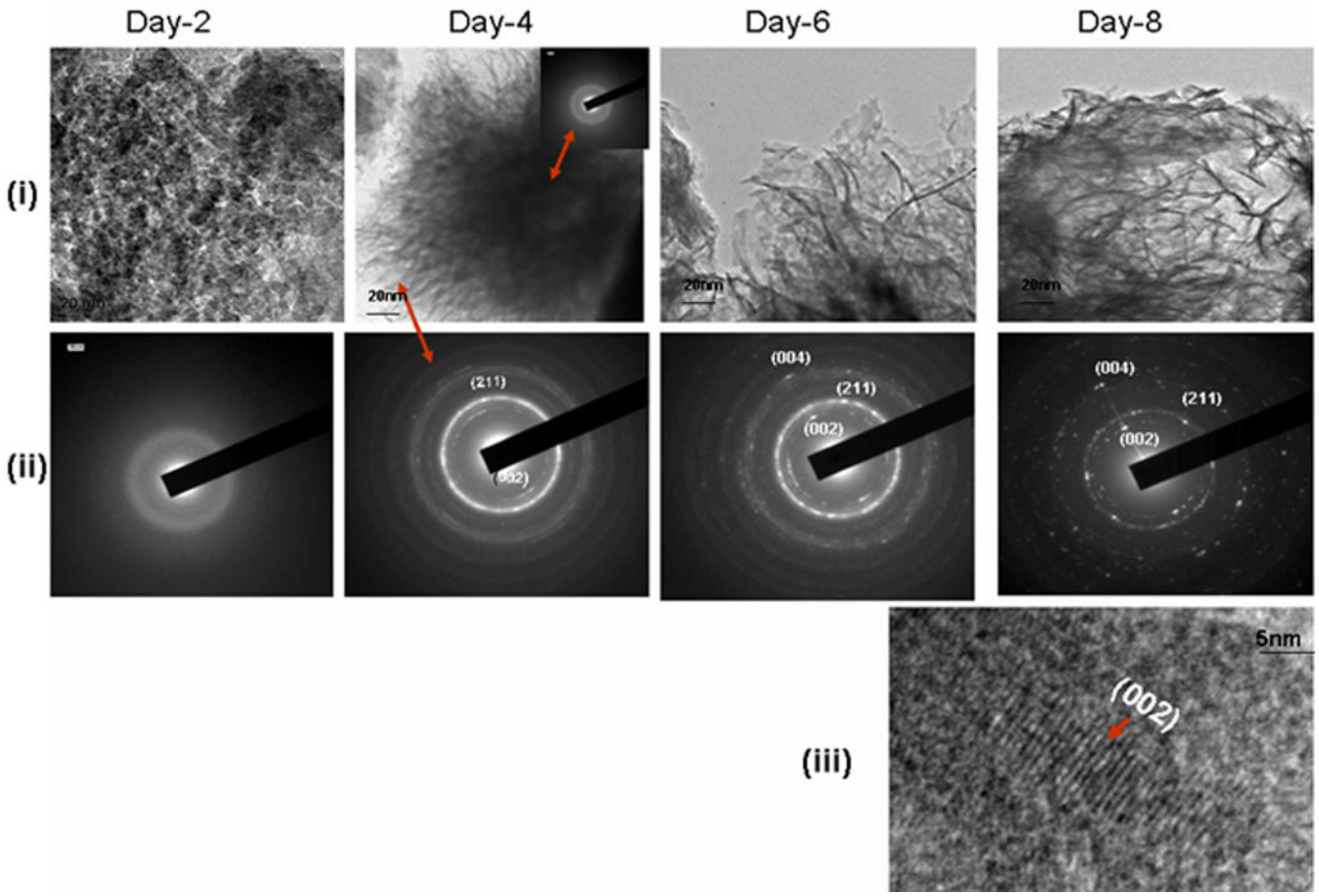

FIG 5B

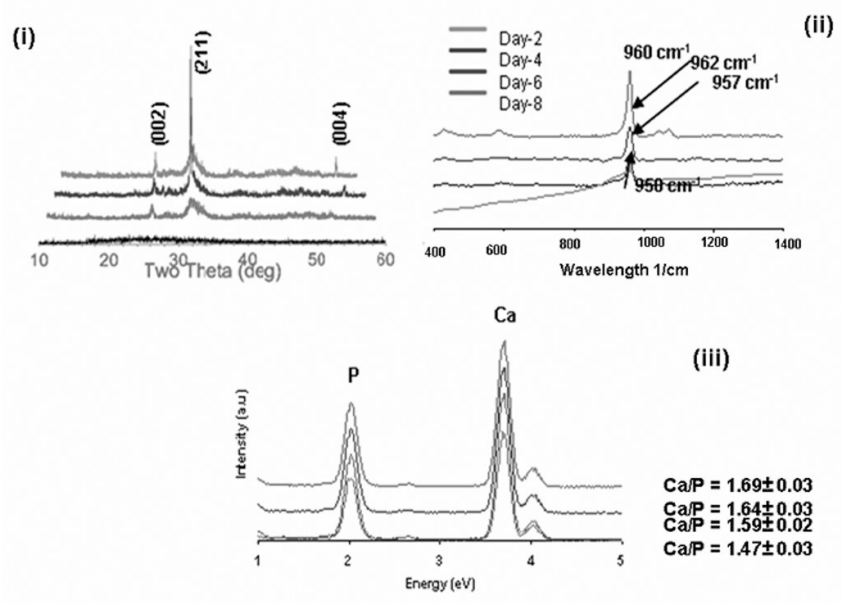

Figure 5.

A: Characterization of the calcium phosphate deposits by TEM (i) Apatite crystallization process characterized by TEM at different days of growth. (ii) Selected Area Electron Diffraction (SAED) of the calcium phosphate deposits obtained at different growth periods, (iii) High resolution TEM showing the lattice spacing of 0.35nm corresponding to the (002) lattice plane of HAP.

B: Characterization of the calcium phosphate deposits by XRD, Raman and EDX: (i) XRD spectra obtained on calcium phosphate deposits obtained after 2,4,6 & 8 days of growth; (ii) Raman spectra obtained on calcium phosphate deposits at 2, 4, 6 & 8 days. Note shift in the wavelength from 950cm^{-1} to 960cm^{-1}; (iii) Energy dispersive X-ray (EDX) spectra showing the Ca/P ratio obtained on calcium phosphate deposits from day 2,4,6 & 8 days of growth.

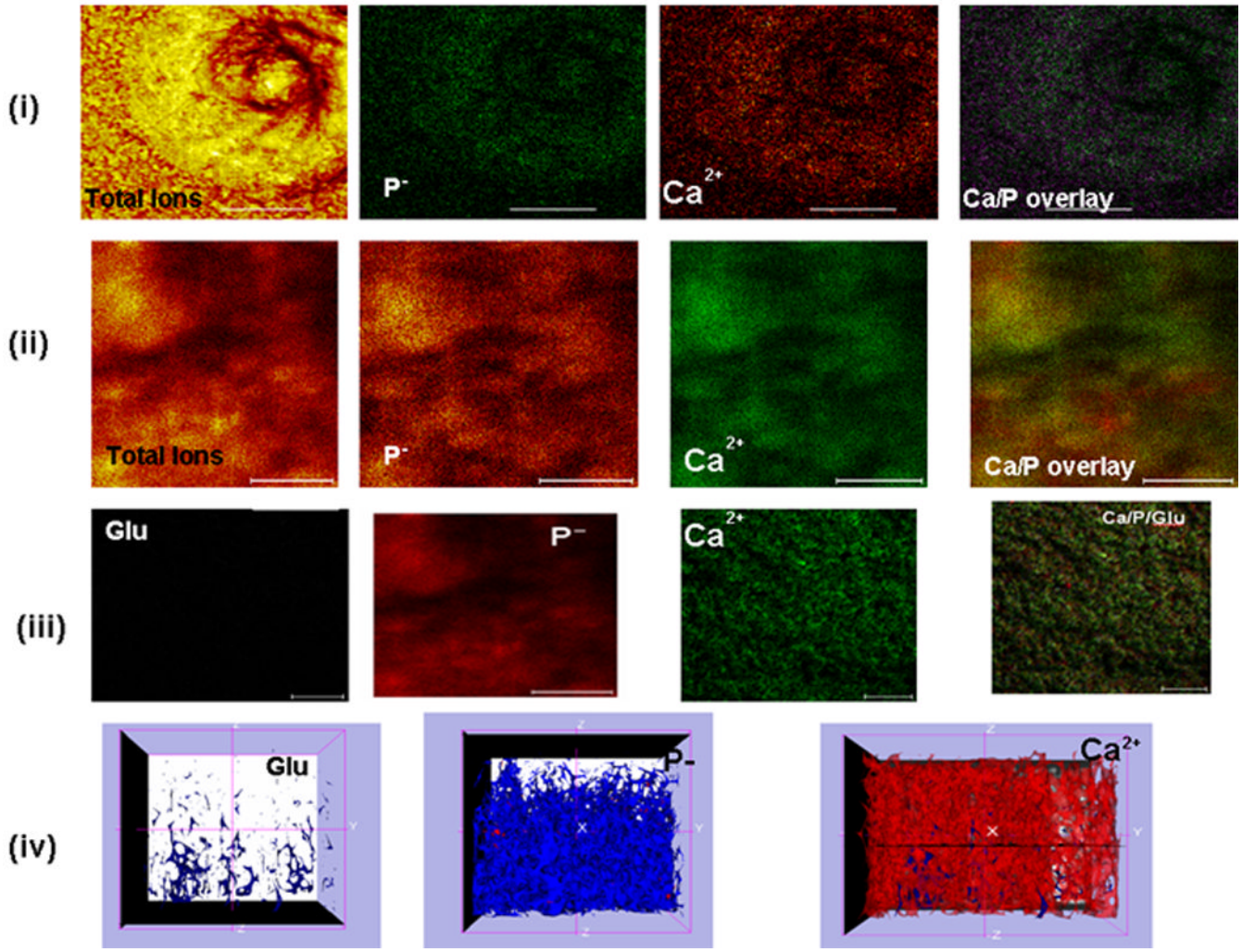

Figure 6. ToF-SIMS analysis of the LZ and LZ-CDMP1 mineralized surface to identify the ion distributions in the mineralized matrix

(i) Topography showing the distribution of calcium and phosphate ions deposited on LZ template after 8 days of growth; (ii) Topography showing the calcium and phosphate ion distribution on LZ-CDMP1 template after mineralization for 8 days. Note the abundance of calcium and phosphate ions; (iii) Predominant ions and amino acid fragment after 1 hour of ion etching on LZ-CDMP1 template. Note the presence of glutamic acid residue in close association with the calcified matrix. (iv) Three dimensional representation of (C) showing the colocalization of glutamic acid along with calcium and phosphate ions. Scale bar for the TOF-SIMS images is 10μm.

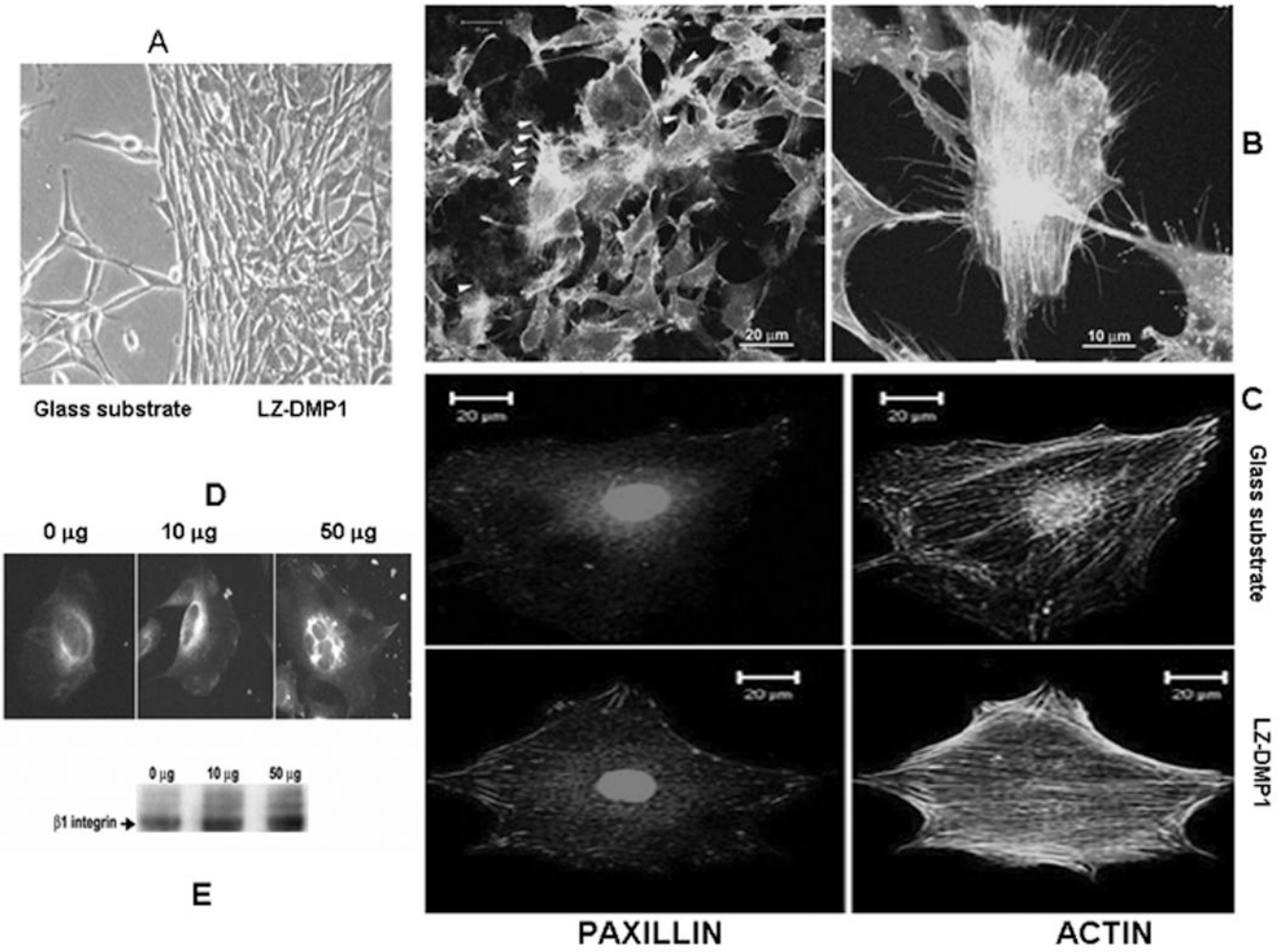

Figure 7. LZ-CDMP1 serves as a template for MC3T3-E1 cell attachment

A: LZ-CDMP1 promotes cell attachment. Numerous filopodia were observed for cells plated on LZ-DMP1. **B & C**: LZ-DMP1 promotes focal adhesion complexes as indicated by activation of paxillin and presence of dense actin stress fibers. **D & E**: Enhanced expression and clustering of β1 integrin when modulated by LZ-CDMP1.